Renewable Energy 119 (2018) 95–105

Contents lists available at ScienceDirect

Renewable Energy

journal homepage: www.elsevier.com/locate/renene

Model test research of a semisubmersible floating wind turbine with an improved deficient thrust force correction approach

Liang Li [a, c], Yan Gao [a, *], Zhiqiang Hu [b, c], Zhiming Yuan [a], Sandy Day [a], Haoran Li [c]

[a] Department of Naval Architecture Ocean and Marine Engineering, University of Strathclyde, 100 Montrose Street, Glasgow G4 0LZ, United Kingdom
[b] School of Marine Science and Technology, Newcastle University, Newcastle upon Tyne, NE1 7RU, United Kingdom
[c] State Key Laboratory of Ocean Engineering, Shanghai Jiao Tong University, Shanghai, 800 Donchuan Road, 200240, China

ARTICLE INFO

Article history:
Received 3 October 2016
Received in revised form
26 October 2017
Accepted 4 December 2017
Available online 5 December 2017

Keywords:
Floating wind turbine
Model test
Thrust force correction approach
Renewable energy
Hydrodynamic load
Aerodynamic load

ABSTRACT

This paper investigates the model test research of a semisubmersible floating wind turbine. An improved method is proposed to correct the deficient thrust force in a Froude-scale experimental condition, which is able to simulate the rotor operational state more realistically by allowing the rotor to rotate freely with the wind. This approach also maintains tip speed ratio to some extent and overcomes previously reported negative effects produced by common correction ways. Reduced platform resonant motions in the presence of wind force are observed. Due to rotor rotation, resonant yaw and roll motions are induced even in heading wind and wave state. Tower vibration is found to be suppressed by the wind force. Multi-frequencies components are observed in the response of tower-top shear force, which is governed by the couplings of hydrodynamic loads, aerodynamic loads and tower vibration. It is also found that the dynamic response of the mooring line is mainly dominated by wave load and aerodynamic effect can be simplified as an extra constant force.

1. Introduction

Due to issues like environmental pollution, energy crisis and sustainable development, the development of wind energy industry has been boosted by the global pursuit of renewable energy. Although the commercial application of onshore wind turbines has been proved successful, the traditional land-based wind turbines are continually complained about the visual, acoustic and environmental impacts. Besides, it is technologically difficult to achieve high energy efficiency from onshore wind resource as a result of turbulent wind farm and low annual mean wind velocity. Therefore, the wind energy industry is trying to exploit the high-quality wind resource in deep water zones.

A series of floating wind turbine concepts have been proposed all over the world. Statoil launched a spar-buoy floating wind turbine project, namely the Hywind concept [1], which is the first full scale floating wind turbine that has ever been built. Roddier et al. [2] made efforts on the feasibility study of the WindFloat concept, a three–column submersible floating foundation for offshore wind turbine [3–5]. Karimirad and Michailides [6] proposed a V-shaped semisubmersible offshore wind turbine. Li et al. [7] studied the dynamic response of a spar type floating wind turbine when incorporated with a wave energy converter and two tidal turbines.

The study of floating wind turbine is multi-disciplinary, involving hydrodynamics, aerodynamics, control algorithm, modeling of structure and multi-body dynamics. Borg and Collu [8] discussed the approach of developing a coupled numerical model for floating wind turbine, considering aerodynamics, hydrodynamics, structural deflection, mooring line dynamics and control scheme. Martin [9] presented detailed information on scaling methodology, design and physical characterization of the NREL's baseline wind turbine for the application in model test. Farrugia et al. [10] studied wave motions effects on wind turbine rotor aerodynamics using lifting line method. Salehyar and Zhu [11] examined the aerodynamic dissipation effect on the wind turbine blades with a quasi-static approach and an unsteady approach, respectively. Larsen and Hanson [12] presented an improved control algorithm to overcome the negative damping caused by blade pitch control for over rated wind velocities. Odgaard et al. [13] used Pareto curves to tune a linear model predictive controller for wind turbines.

Based on the development of basic principles, simulation tools are proposed for the fully coupled analysis of floating wind

* Corresponding author.
E-mail address: yan.gao@strath.ac.uk (Y. Gao).

https://doi.org/10.1016/j.renene.2017.12.019
0960-1481/

turbines. Jonkman [14] developed a hydrodynamic module and implemented it to FAST. Skaare et al. [15] came up with a new computational tool on the basis of aerodynamic code HAWC2 and hydrodynamic, structural and control system analysis tools SIMO/RIFLEX. Li et al. [16] developed a aero-hydro dynamic code for analysis of floating wind turbine. Quallen and Xing [17] developed a simulation tool with a variable-speed generator-torque controller using CFD calculation method.

Although a series of simulation tools have been developed, the validations of these tools still rely on comparative code-to-code check analysis due to the lack of reliable model test results. The validation work based on model test method has not been adequately conducted. With the collaboration of a group of research institutes, including NREL, MAINE University and MARIN etc., projects OC3 and OC4 started the steps of validating numerical tools and also obtaining floating wind turbine's dynamic characters through the technique of basin model test [18,19]. Duan et al. [20] investigates the dynamic response of a spar-buoy floating wind turbine with model test approach. Nevertheless, few test data are open to the public and researchers usually find it difficult to validate their in-house numerical codes.

Model test technique provides not only a reliable source to validate numerical analysis codes, but also a good approach to demonstrate the dynamic characters of the floating system, especially those unable to be captured by numerical simulations. For the purpose of fully studying the dynamic response of floating wind turbine and also providing model test results for the validation of numerical codes, a model test research for a 5 MW wind turbine is conducted in Shanghai Jiao Tong University. Firstly, the set-up of the model test is presented. Identification test results are given subsequently to calibrate the floating wind turbine model and the environmental conditions. Afterwards, the experimental data for various test cases are presented to demonstrate the dynamic characters of the floating wind turbine. Finally, conclusions drawn from the model test research are presented.

2. Model test set-up

To fully understand the response mechanism of floating wind turbine under hydrodynamic and aerodynamic excitations, a large-scale model test program is launched in the Deepwater Offshore Basin at Shanghai Jiao Tong University. The water basin, equipped with advanced wave-generating system, current-generating system, wind-generating system and other testing facilities, is 50 m in length, 40 m in width and 10 m in depth. The model test is conducted at a Froude scale of 1:50. The water depth is set as 4 m corresponding to the full-scale depth of 200 m. As shown in Fig. 1, the OC4-DeepCwind concept [21] is used in the test. Nevertheless, some modifications for the floating foundation and the mooring system are made due to the restrictions caused by turbine model manufacturing and installation of data measurement devices.

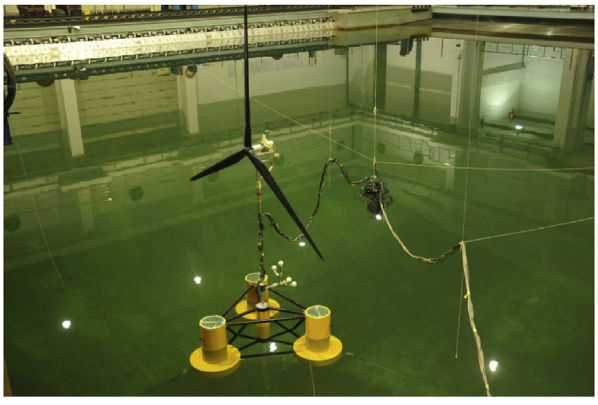

Fig. 1. Model of semisubmersible floating wind turbine.

2.1. Scaling methodology and deficient thrust force correction approach

Both hydrodynamics and aerodynamics should be regarded as dominating factors in the model test research of a floating wind turbine. Froude number similitude is typically employed in water basin test to ensure the relationship between inertial and gravitational wave forces. Meanwhile, Reynolds number similarity is more common in wind tunnel test as it preserves the relationship between viscous and inertial forces of incident flow. It is ideal to maintain Froude number and Reynolds number similitude simultaneously in the test. From a practical perspective of view, however, it is impossible to achieve such a goal. Therefore, a priority of the two scaling schemes should be selected. In a water basin test, a Froude-scaled model is able to cover most of the crucial properties which govern the dynamic responses of a floating body in waves. It is straightforward to employ the hydrodynamic view and maintain the Froude number in the test program. Therefore, both the floating wind turbine model and the incident waves are scaled with Froude number similitude in the model test.

As Froude scale method is applied in the model test, the Reynolds number similitude is no longer satisfied and the aerodynamic performance of the wind turbine will change. To demonstrate Reynolds number effect, XFOIL [22] is used to calculate the lift coefficient C_L and drag coefficient C_D of the blade airfoil at full scale ($\mathrm{Re} = 1.15 \times 10^7$) and model scale ($\mathrm{Re} = 3.25 \times 10^4$), respectively (see Fig. 2). The results show that C_L is reduced whereas C_D is increased at the model scale compared with prototype design. The thrust force coefficient C_T is subsequently computed with FAST [23] and the results are displayed in Fig. 3. Apparently, the model scale thrust force is much lower than the prototype value if no correction approach is applied.

Most correction methods are based on increasing the model scale wind speed while utilizing an electric motor to drive the rotor. In this way, rotor speed can be exactly tuned and the designed thrust force is obtained by increasing wind speed massively. However, the TSR is no longer maintained, which ensures that the system excitation resulting from rotor imbalance or aerodynamic interaction with the tower will possess the correct frequency [24]. This type of correction method may also lead to undesirable force on the tower and the platform hull above water surface since the wind speed is significantly increased [9]. Besides, the generator is not simulated properly as it drives the rotor rather than being driven by the rotor. In the test program, we introduce an improved approach to acquire the designed thrust force and better simulate the generator operation state. Instead of being driven by an electric motor, the rotor is purely driven by the wind. The electric motor is merely used to represent the wind turbine generator. By adjusting the wind speed gradually, the thrust force acting on the rotor is recorded. The adjusting of rotor speed is achieved by an appropriate selection of the motor among several available motors with different resistance properties. In this way, the TSR can be tuned although not exactly. After a series of tests, the most favorable motor is selected and the measured relationships between thrust force, wind speed, rotor speed and TSR are outlined in Table 1. It should be noted that the relationships in Table 1 will differ when a different motor is used.

The improved correction method possesses several advantages over common ways. It is capable of simulating operation state of the rotor realistically. In model test, the relative wind speed keeps

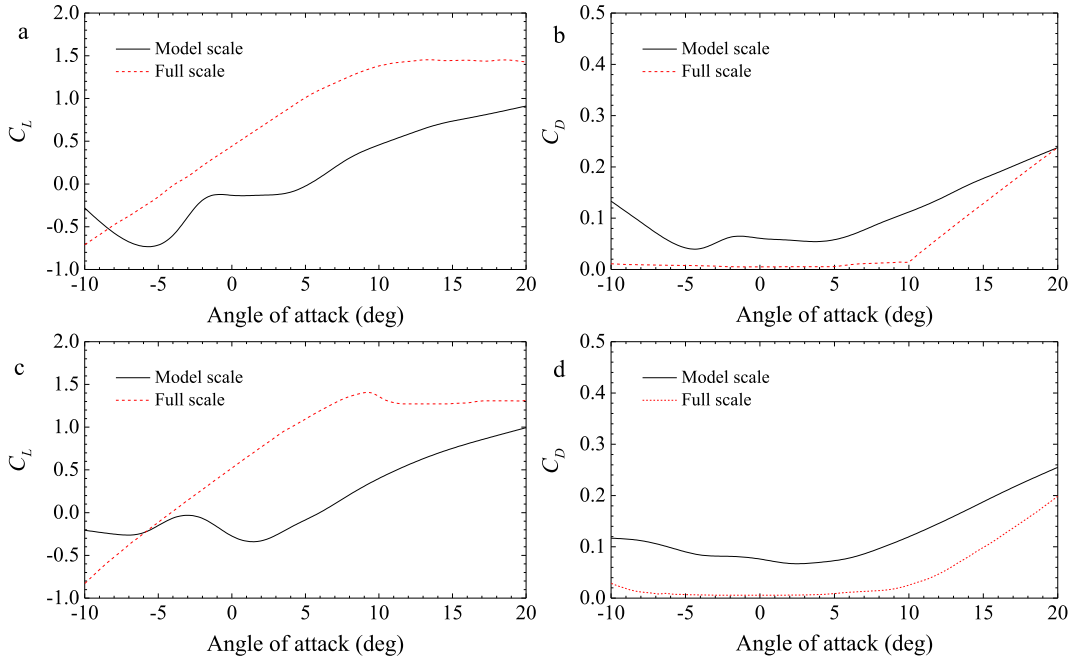

Fig. 2. Aerodynamic performance of blade airfoil at full scale and model scale. (a) C_L, NACA64_A17; (b) C_D, NACA64_A17; (b) C_L, DU21_A17; (b) C_L, DU21_A17.

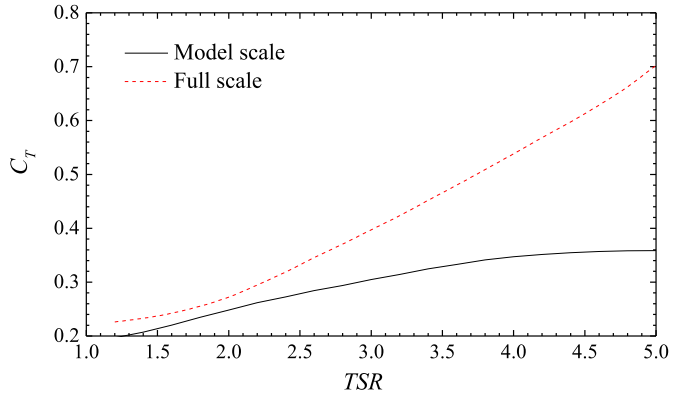

Fig. 3. Variation of thrust force coefficient with respect to tip speed ratio (TSR), blade pitch angle is fixed at 0 deg.

Table 1
Relationship between thrust force, wind speed and rotor speed.

Rotor thrust (kN)	Prototype			Measurement		
	Wind speed (km/hr)	Rotor speed (rpm)	TSR	Wind speed (km/hr)	Rotor speed (rpm)	TSR
276	18	7.5	9.98	33.8	7.9	5.59
494.9	28.8	9.3	7.73	41	11.2	6.53
770.4	41	12.1	7.06	46.1	14.1	7.32
451.1	64.8	12.1	4.47	40	10.9	6.53
388.9	82.8	12.1	3.50	39	10.6	6.47
145	144	0	0	56.5	0	0

varying with platform motions and thus the rotor speed changes accordingly. It is consistent with realistic situation since the control system is active for a full scale floating wind turbine during operational condition. Besides, the shaft axial torque obtained in the model test is more reasonable compared with that acquired by common corrections ways. This is because the shaft axial torque is purely wind-driven rather than being generated by the motor. By adopting this free rotation approach, it is also able to acquire the designed thrust force without increasing the wind speed significantly. For example, the wind speed is increased from 41 km/h to 74.9 km/h to match the rated thrust force in the work of Martin et al. [24] while the increased wind speed is just 46 km/h in our test. In this way, the undesirable excess drag on non-rotor structures is reduced. Furthermore, it maintains the TSR to same extent. Although the rotor speed is determined by the wind and cannot be adjusted exactly in the test, it is shown that the rotor speed changes slightly due to the appropriate selection of the motor. For example, the measured rotor speed is 14.4 rpm compared with designed value 12.1 rpm in rated thrust case.

2.2. Model description

2.2.1. Wind turbine

The wind turbine in the test is based on NREL's 5 MW baseline wind turbine [25]. The measured scantlings of turbine model are compared with prototype values in Table 2.

The blades are manufactured according to geometric similitude with prototype (see Fig. 4). As Froude scale scheme is adopted in the test, the mass of each blade is required to be kept at only 134 g. From a practical perspective, it is a major challenge in the test program. Woven carbon fiber material is used to meet the scaled

Table 2
Mass and CM (center of mass) location of main components of wind turbine.

Item	Prototype		Measurement	
	Mass (kg)	CM (m)	Mass (kg)	CM (m)
Blades	53,220	90	52,659	90.65
Hub	56,780	90.17	57,272	90.65
Nacelle	240,000	89,35	232,291	90.65
Tower	249,718	43.4	287,128	51
4 Identical lamps at tower bottom	–	–	27,163	30.9
1 identical lamp at tower top	–	–	6791	92.15
Instrumentation cables	–	–	86,228	57.1
Total Wind turbine	599,718	70.35	749,532	69.45

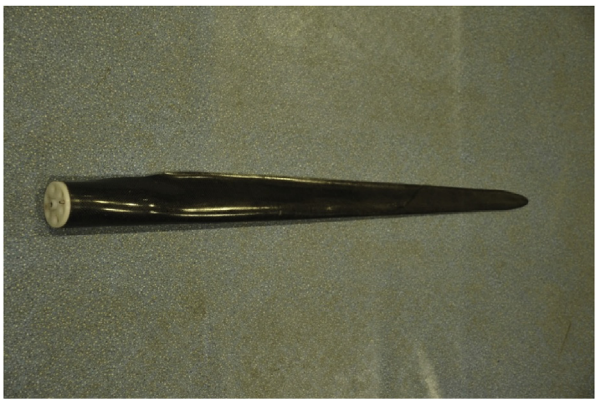

Fig. 4. Blade model.

mass target. To avoid accidental events such as blades-tower collision and get rid of the aero-elastic coupling, bracing components are installed inside to make the blade rigid and prevent any blade deflection. An electric motor is installed at the tower-top to represent the nacelle drive-drain system and the generator. As discussed above, no power is supplied to the motor and it is purely driven by wind. As no control device is implemented in the test, blade-pitch angle is kept at 0° for operational cases and 90° for parked cases, respectively. The shaft tilt is set 0° in the test program, instead of prototype value 5°.

2.2.2. Platform

The floating foundation is made up of three main offset columns inducing buoyance and restoring force, one central column supporting the wind turbine, as well as a series of diagonal cross and horizontal bracing components. In order to a gain good hydrostatic stability performance, a ballast tank is installed at the bottom of each main offset column. The main scantlings of the platform are listed in Table 3.

2.2.3. Mooring system design

The floating wind turbine is moored at sea site with a water depth of 200 m, through a mooring system composed of three taut catenary lines. Fairleads are connected to the tops of ballast tanks. Fig. 5 illustrates the coordinate system in the test. The three mooring lines are oriented symmetrically at 60°, 180°, and 300° about the vertical axis. The relevant properties of mooring lines are outlined in Table 4.

Table 3
Main scantlings of the platform.

Term	Value
Depth of platform base below SWL	20 m
Elevation of platform top above SWL	10 m
Elevation of offset columns above SWL	12 m
Spacing between offset columns	50 m
Length of upper columns	26 m
Length of base columns	6 m
Depth to top of base columns below SWL	14 m
Diameter of main column	6.5 m
Diameter of offset (upper) columns	12 m
Diameter of base columns	24 m
Platform mass	12,912,500 kg
Displacement	13,986.8 m^3
CM below CWL	13.5 m
Platform roll inertia (about CM)	6.052×10^9 kg m^2
Platform pitch inertia (about CM)	6.052×10^9 kg m^2
Platform yaw inertia (about CM)	1.201×10^{10} kg m^2

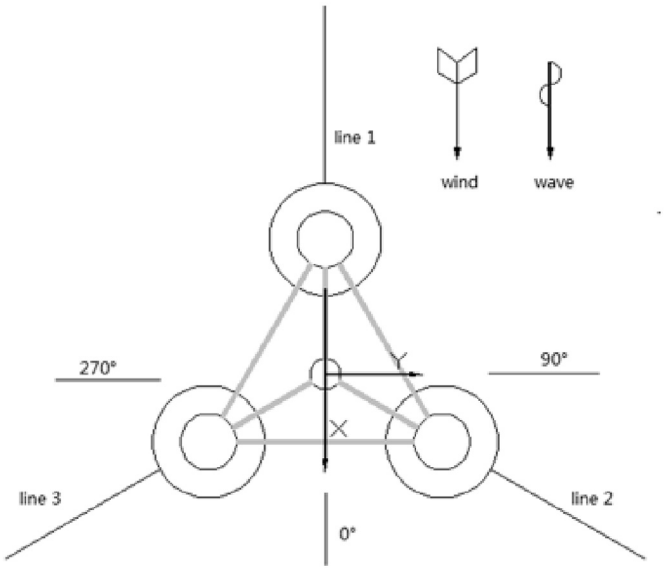

Fig. 5. Coordinate system and mooring system configuration.

Table 4
Mooring system properties.

Term	Value
Number of mooring lines	3
Angle between adjacent lines	120°
Depth to anchors	200 m
Depth to fairleads	14 m
Radius to anchor	853.7 m
Radius to fairleads	40.868 m
Unstretched mooring line length	835.5 m
Mooring line diameter	0.0766 m
Equivalent line mass density	113.35 kg/m
Equivalent mooring line extensional stiffness	753.6 MN

2.3. Data measurement

Advanced data acquisition techniques are used to measure the dynamic response of the floating wind turbine model. Data collection transducers are shown in Fig. 6. Motions of the nacelle and the platform are captured with a non-contact optical tracking system, which is mainly composed of positive identical lamps and capturing cameras. Tension transducers are connected to the fairleads to collect mooring line tension signal. Two sets of load cells are installed. 1# load cell is installed between the nacelle and the tower structure to measure the shear force and bending moment applied at this position; and 2# load cell is installed in the rear part of the nacelle to collect the shaft axial force data. Besides, an accelerometer is also installed to measure the nacelle acceleration. Wave probes are used in the study to record time series of wave elevation. Data collection frequency is set to 20 Hz for all sensors in each loading case. A summary of the data recorded in the test is listed in Table 5.

3. Identification test results

Prior to the basin test, a series of identification test cases are conducted. At first, the spatial homogeneity and turbulence of the generated wind field are checked. Hammer test is also performed to estimate the vibration frequency of the tower. Mooring system calibration and free decay test are followed to identify the natural periods of the floating system.

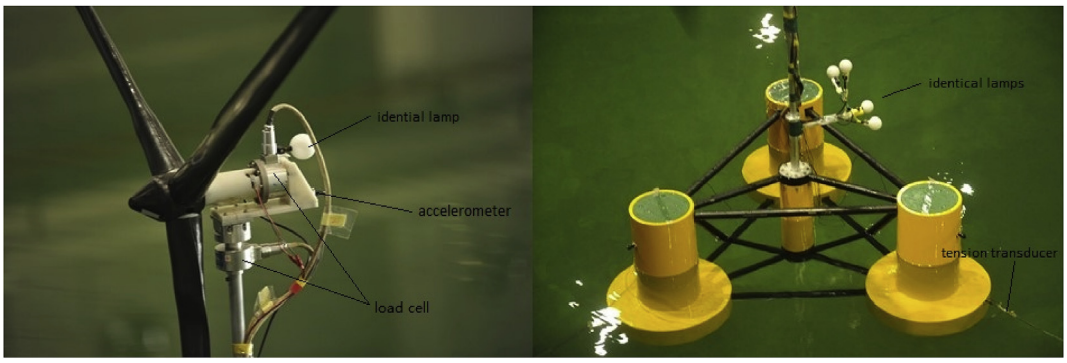

Fig. 6. Illustration of the data collection devices.

Table 5
Summarization of data acquisition.

Term	Location	Recorded data
Load cell	Nacelle	Shaft axial force and torque
	Tower-top	Shear force and bending moment
Accelerometer	Nacelle	Nacelle acceleration
Optical motion capture system	Nacelle	Nacelle motion
	Platform	Platform motion
Tension transducer	Fairlead	Mooring line tension force
Wave probes	Surroundings	Wave elevation

3.1. Calibration of wind field

Calibration test is conducted on the land to estimate the generated wind field quality. A series of thermal wind speed probes are installed in front of the wind generator to form a spatial matrix and measure the spatial distribution of wind speed in the virtual rotor plane, which is 3 m away from the wind generator. Figs. 7 and 8 illustrate the measured wind field for rated thrust force case. Detailed calibration procedures of the generated wind field can be found in Ref. [26].

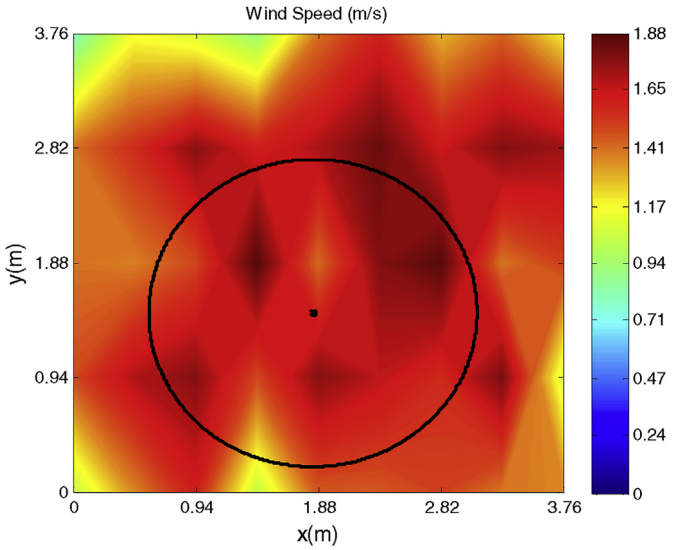

Fig. 7. Wind speed distribution of wind field.

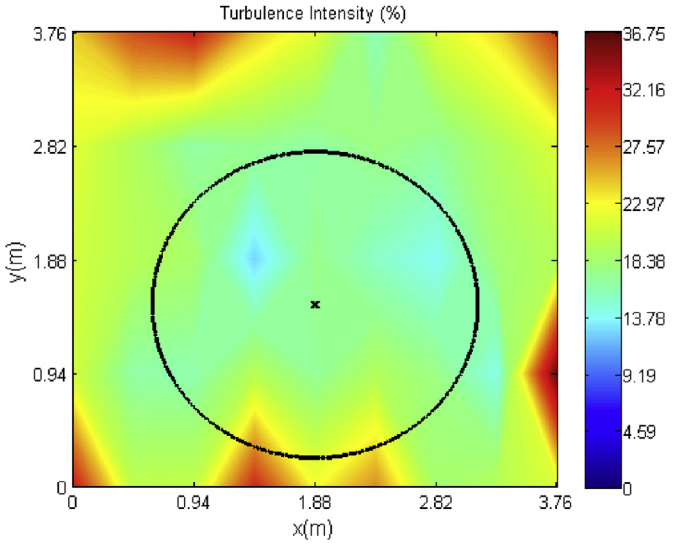

Fig. 8. Turbulence density of wind field.

3.2. Hammer test

The vibration frequency of the tower is measured by hammer test. The tower (without nacelle and rotor) is rigidly connected to the land via a load cell to record the vibration-induced bending moment. An impulse excitation is afterwards applied to the tower-top causing it to vibrate freely. Since the tower is axial symmetric, only fore-aft impulse test is carried out. Hammer test result is illustrated in Fig. 9. The response peak is observed at 2.58 rad/s and 4.21 rad/s, respectively.

3.3. Mooring system horizontal stiffness test

Due to rotor rotation, the platform moves not only in longitudinal direction, but also in transversal direction. Therefore, the mooring line stiffness along both longitudinal and transversal directions are measured. Fig. 10 plots the measured horizontal stiffness.

3.4. Free decay test

Natural periods of the floating system are identified with free decay test. The results of free decay test are listed in Table 6. The time series of decay motions are plotted in Fig. 11.

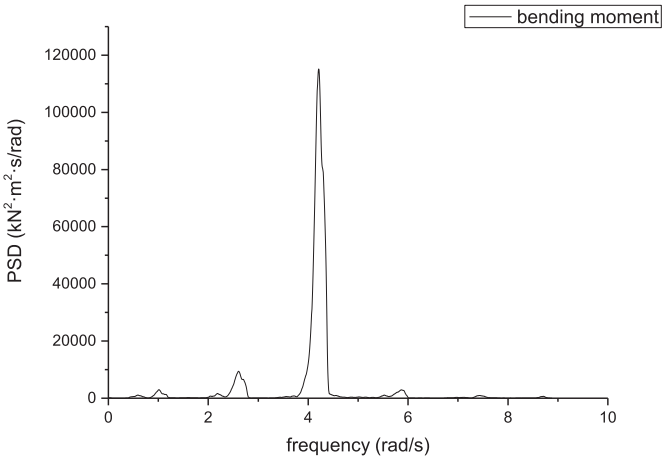

Fig. 9. Hammer test results.

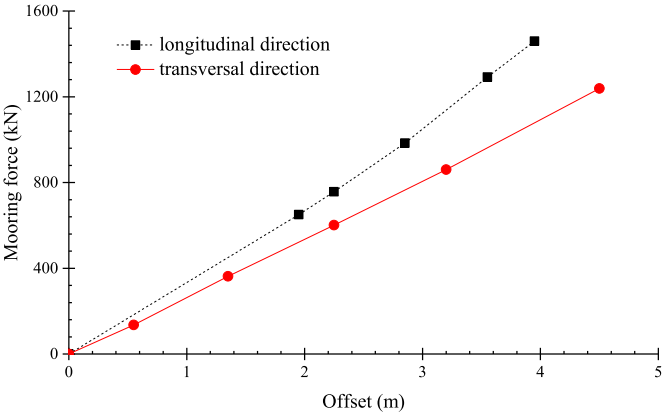

Fig. 10. Measured mooring horizontal stiffness.

Table 6
Results of free decay tests.

	Term	Surge	Heave	Pitch	Yaw
Decay test	Natural period (s)	54.546	16.390	24.492	48.225
	Damping ratio	0.0668	0.0341	0.0622	0.0285

4. Dynamic response of the system

In the experiment program, a set of test cases are conducted to investigate platform motions, structural response and mooring line tension of the floating wind turbine. Firstly, motion response characteristics of the system are analyzed. Aerodynamic effects on platform motions and nacelle accelerations are clarified. Roll and yaw motions induced by rotor rotation are also studied. Secondly, the response mechanisms of shaft axial force and tower-top shear force are investigated. Finally, the tension force of a selected mooring line is analyzed. Table 7 presents a summary of the environmental conditions considered in the test program. The model scale duration of each test case is set 8.5 min, corresponding to full scale 1 h. Both wind and waves are set to propagate along the heading direction in all test cases (See Fig. 5).

4.1. Platform surge and pitch motion characters

The platform motions under various environmental conditions are investigated. As surge and pitch are critical degrees of freedom (DOF) for a floating wind turbine, this section will only deal with the two DOFs. Table 8 lists the statistical results of surge and pitch motions measured in test cases LC1, LC2 and LC3.

The statistical results show that platform motions are greatly influenced by the wind force. With below-rated thrust force acting on the rotor, the mean pitch position is 3.153 deg and this value increases to 4.188 deg when the system is subject to rated wind force. With respect to surge motion, similar conclusion can be obtained. Mean surge position is pushed to 2.747 m with rated thrust force whereas it is just 0.225 m in LC1. Furthermore, it points out that the standard deviations of surge and pitch motions are both somewhat reduced by the wind force. To further investigate platform motions under wave & wind excitations, the time-series of platform motions are analyzed with fast Fourier transform (FFT) method to obtain the power spectrum density (see Fig. 12).

With consideration of the wind force, the resonant motions of surge and pitch are reduced significantly while little change is observed around the wave energy frequency range. Motions are observed within range from 0.4 rad/s to 0.9 rad/s, which are mainly wave-induced and hardly influenced by aerodynamic load regardless of wind speed. It is thus proved that aerodynamic load has a limited influence on the wave frequency motions. Besides, strong response can be observed around the resonant frequency for both surge and pitch motions. Although aerodynamic load plays a tiny role on the wave frequency response, it nevertheless has a significant damping effect on the resonant response. Comparisons between case LC1, LC2 and LC3 manifest that wind force reduces the platform motions and such aerodynamic damping effect is mostly effective around the resonant frequency range.

4.2. Nacelle acceleration

Mechanical facilities installed inside the nacelle will bear inertial loads caused by nacelle accelerations. In the model test, nacelle accelerations along three directions are measured and statistical results of the recorded data are summarized in Tables 9–11.

Although the resonant motions of surge and pitch are reduced in the presence of wind force, the nacelle accelerations seem to be amplified by the wind force. As summarized in Table 9, the maximal value, the mean value and the standard deviation of nacelle acceleration are all somewhat augmented with the increase of wind speed. Acceleration in Y direction is also observed. As shown in Table 10, the standard deviation in case LC3 is about 8 times larger than that in case LC1. Such significant augment of standard deviation inherently implies the excitation of platform sway motion, which will be discussed in more detail in the following part of this paper. Although the wind mainly induces horizontal load, acceleration along vertical direction is still increased in Table 11 due to the coupling between pitch and heave. The statistical results indicate that large wind load is likely to cause significant nacelle acceleration. In order to present the characteristics of the accelerations more clearly, the power spectrum density (PSD) of nacelle accelerations along X direction in the three test cases are shown in Fig. 13.

In parked condition (LC1), it is wave force and tower structural vibration that dominate the nacelle acceleration. According to LC1 curve, the nacelle acceleration is mainly excited by linear wave force and a majority of response energy concentrates on the wave energy frequency range. Another response peak is observed around

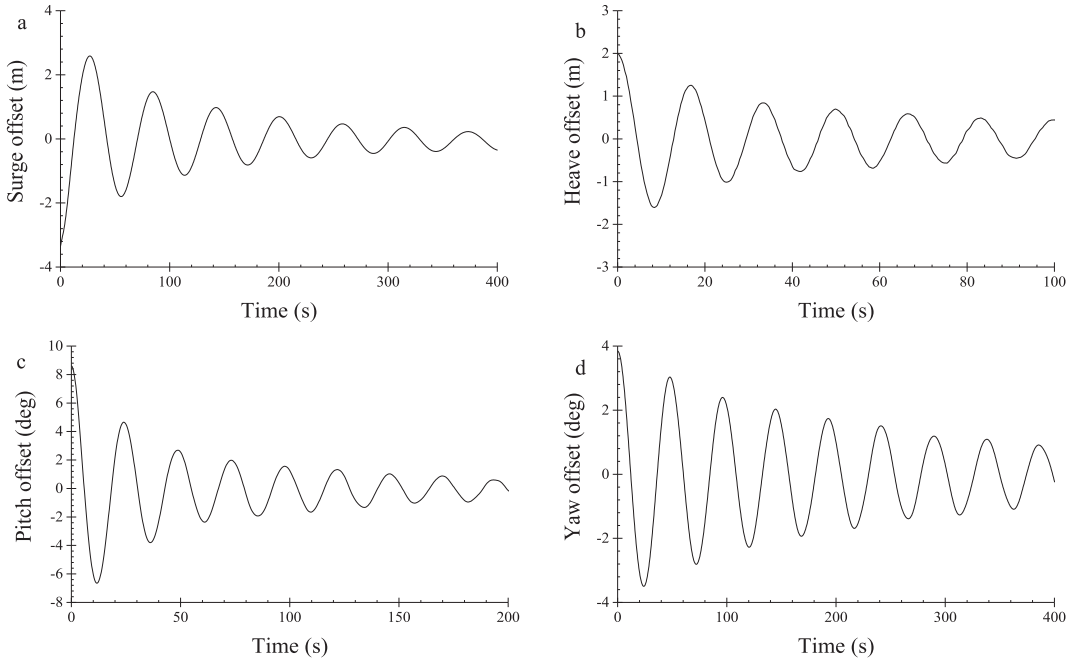

Fig. 11. Free decay motions. (a) Surge motion; (b) heave motion; (c) pitch motion; (d) yaw motion.

Table 7
Environmental condition definition.

Case No.	Wind speed (km/hr)	Rotor speed (rpm)	Wave		
			Hs (m)	Tp (s)	ɣ
LC1	0	0	6	10	2.87
LC2	41	11.2	6	10	2.87
LC3	46	14.4	6	10	2.87
LC4	0	0	2	8	3.3
LC5	46	14.4	2	8	3.3

Table 8
Statistical results of platform surge and pitch motions.

Case No.	Degree of Freedom	Max	Min	Mean	Std. dev.
LC1	Surge (m)	2.709	−1.663	0.225	0.690
	Pitch (deg)	3.330	−1.946	0.369	0.620
LC2	Surge (m)	4.652	0.301	2.137	0.651
	Pitch (deg)	5.648	1.253	3.154	0.508
LC3	Surge (m)	5.209	0.898	2.747	0.647
	Pitch (deg)	6.790	2.346	4.188	0.537

0.27 rad/s, which is close to pitch resonant frequency. Apart from hydrodynamic excitations, the vibration of tower also stimulates the nacelle acceleration. LC1 curve shows a substantial response peak at 2.68 rad/s, which is close to the tower vibration frequency obtained by hammer test.

When the wind force is considered, a couple of extra frequency components appear in the response. In addition to the response induced by wave force and tower vibration, the nacelle acceleration is significantly excited around 3P rotor rotation frequency. As discussed above, the rotor is purely driven by wind and the rotor speed keeps varying due to platform motions. Therefore, the 3P rotation frequency in Fig. 13 is somewhat different from that in Table 1. For LC2 and LC3 PSD curves, it can be seen that response amplitudes around pitch resonant frequency and tower vibration frequency are substantially reduced. It inherently manifests that pitch motion and tower vibration are suppressed. On the contrary, the nacelle acceleration is amplified around wave energy frequency range with the consideration of wind force.

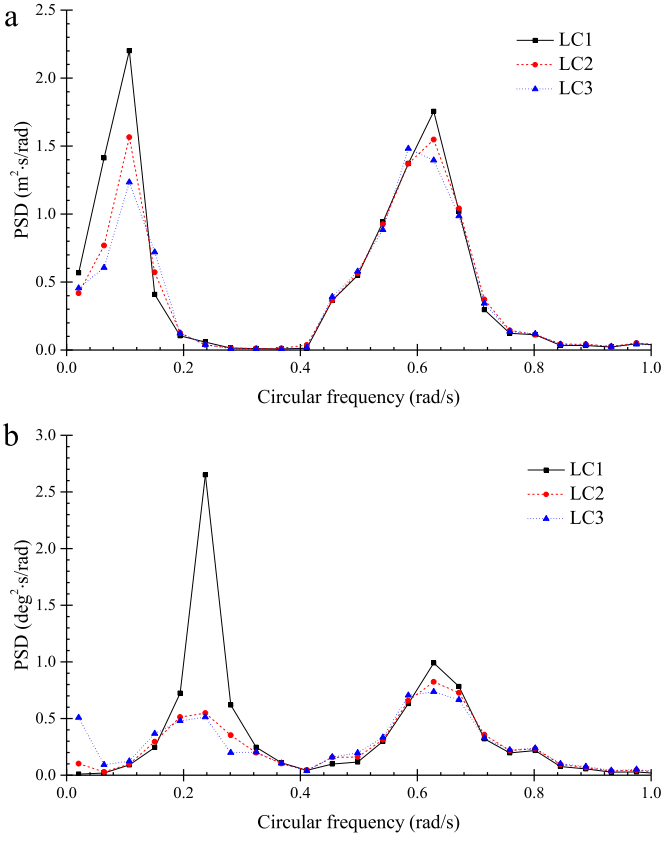

Fig. 12. Power spectrum density of platform motions. (a) Surge motion; (b) pitch motion.

Table 9
Statistical results of nacelle acceleration along X direction.

Case No.	Max (m/s^2)	Min (m/s^2)	Mean (m/s^2)	Std. dev. (m/s^2)
LC1	1.752	−1.760	0.047	0.389
LC2	2.360	−1.222	0.583	0.451
LC3	2.573	−1.020	0.785	0.476

Table 10
Statistical results of nacelle acceleration along Y direction.

Case No.	Max (m/s^2)	Min (m/s^2)	Mean (m/s^2)	Std. dev. (m/s^2)
LC1	0.22	−0.123	0.05	0.047
LC2	1.239	−1.092	0.063	0.25
LC3	1.544	−1.495	0.073	0.38

Table 11
Statistical results of nacelle acceleration along Z direction.

Case No.	Max (m/s^2)	Min (m/s^2)	Mean (m/s^2)	Std. dev. (m/s^2)
LC1	0.489	−0.396	0.021	0.121
LC2	1.086	−1.044	0.027	0.223
LC3	1.077	−1.386	0.042	0.27

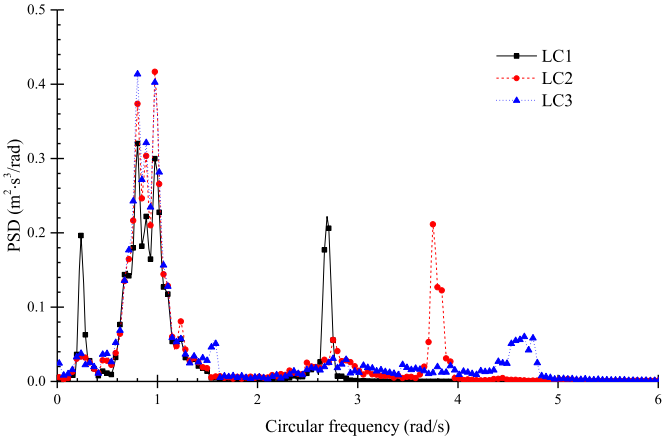

Fig. 13. Power spectrum density of nacelle acceleration along X direction.

4.3. *Effects of rotor rotation on yaw and roll motions*

Simulation cases LC4 and LC5 are selected to clarify the rotor rotation effect on platform motions. The wind turbine is parked in LC4 whereas the wind drives the rotor to rotate in LC5. As shown in Fig. 14, the floating system is subject to an extra torque which is induced by the rotor. Due to pitch motion, the rotor torque is separated into a vertical component and a horizontal component. The vertical component induces gyroscopic loading and excites yaw motion while the horizontal component will lead to roll motion. Apparently, the two components vary with time and are governed by both incident wave frequency and pitch natural frequency of the floating system.

As listed in Table 12, the standard deviation of yaw motion in LC5 is nearly doubled compared with that in LC4. Besides, the mean position of yaw motion is kept at 0.157 deg with gyroscopic loading in LC5. It is caused by the non-zero average vertical torque components associated with inclined mean position of the platform. Rotor rotation effect is mostly effective on the resonant response of yaw motion (see Fig. 15). Due to the symmetry geometry of the platform, yaw motion is seldom observed in LC4. Comparatively,

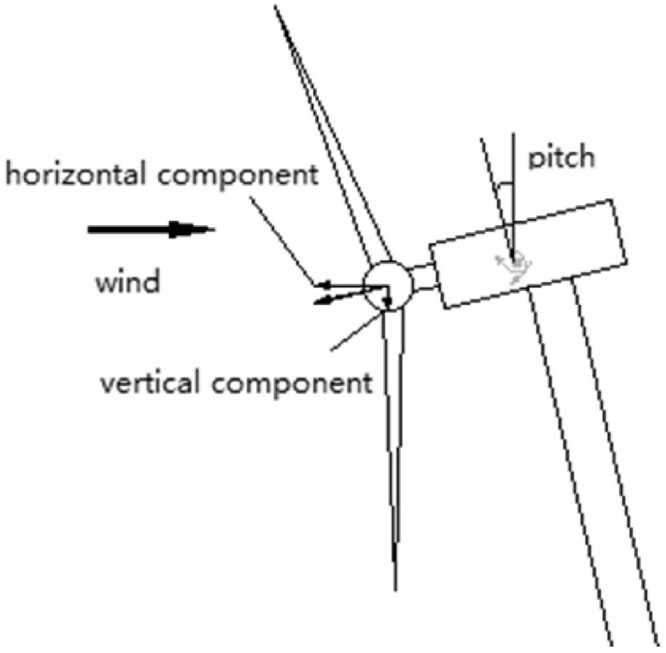

Fig. 14. Horizontal and vertical components of rotor torque.

Table 12
Statistical results of yaw motion.

Case No.	Max (deg)	Min (deg)	Mean (deg)	Std. dev (deg)
LC4	0.321	−0.189	0.089	0.071
LC5	0.561	−0.311	0.157	0.127

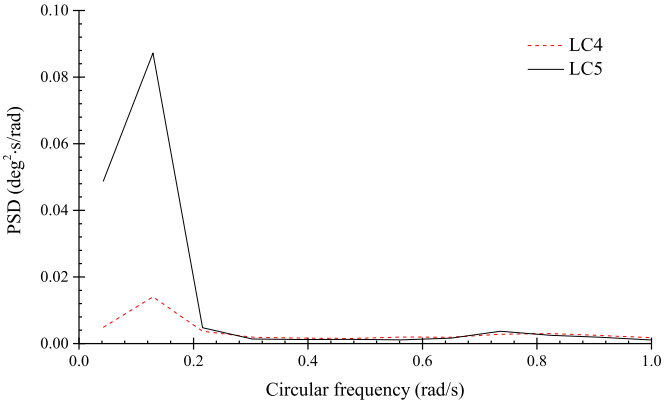

Fig. 15. Power spectrum density of yaw motion.

yaw motion is excited significantly at about 0.14 rad/s by the gyroscopic loading, which is close to yaw natural frequency. Apart from inducing yaw motion, gyroscopic loading causes some unfavorable yaw bearing at the connection of the nacelle and the tower. The power spectrum density of yaw bearing at this connection position is displayed in Fig. 16. Although yaw motion is excited at its resonant frequency, it is interesting to find that the peak response of the yaw bearing is at 1.58 rad/s, which is close to the rotor rotation speed. It manifests that the yaw bearing is mainly induced by wind force.

Similar to the gyroscopic loading, the horizontal component of the rotor torque will induce unfavorable roll motion as well. What's more, the resonant roll motion may be excited since the varying

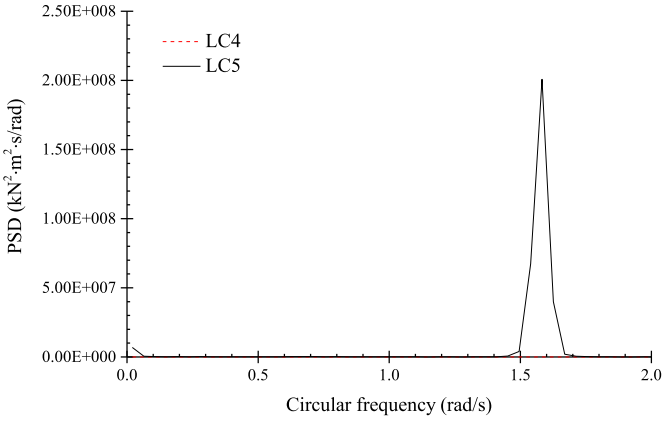

Fig. 16. Power spectrum density of tower-top axial torque.

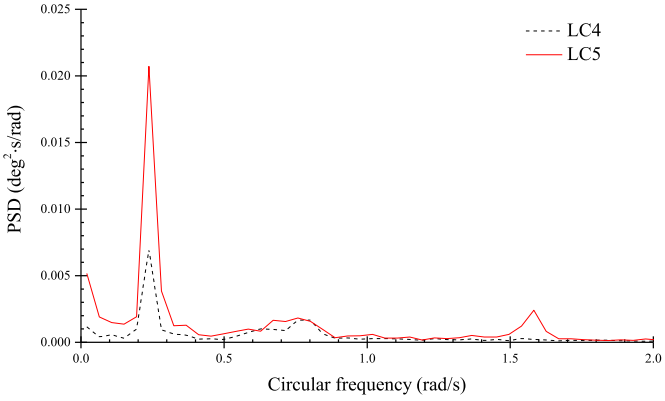

Fig. 17. Power spectrum density of roll motion.

frequency of the horizontal component is very close to roll resonant frequency. Fig. 17 displays the power spectrum density curves of platform roll motion. It is shown that the resonant roll motion is excited by the horizontal the rotor torque. Besides, low-frequency roll motion is observed due to the coupling between roll and sway motions.

4.4. Shaft axial force

The measured shaft axial force consists of two components, namely the wind force applied on the rotor plane and the inertial force induced by the nacelle motions. Statistical results of the shaft axial force are summarized in Table 13. Alongside with the increase of wind force, the maximum, the minimum and the mean values of shaft axial force are all increased where just a little bit augment of the standard deviation is observed. It seems that the shaft axial force is mainly dominated by the inertial motions of the nacelle and wind force can be simplified as a constant linear superposition.

Fig. 18 displays the frequency components of shaft axial force in the three test cases. When the wind force is not considered,

Table 13
Statistical results of shaft axial force for LC1, LC2 and LC3.

Case No.	Max (kN)	Min (kN)	Mean (kN)	Std. dev (kN)
LC1	377.202	−478.436	41.699	98.686
LC2	1068.2	166.6	651.7	107.506
LC3	1334.76	506.562	909.342	117.6

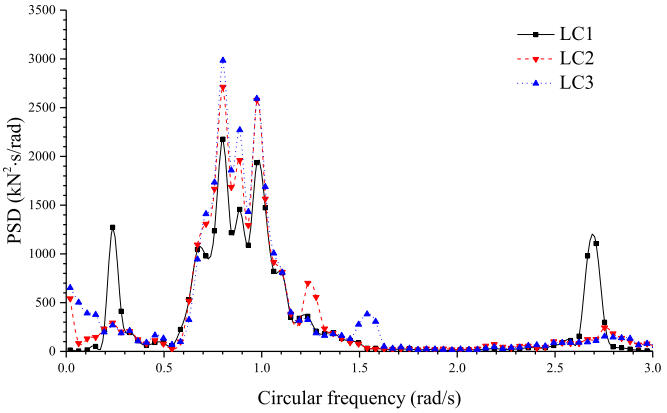

Fig. 18. Power spectrum density of shaft axial force.

response peak can be found at pitch resonant frequency, wave frequency and vibration frequency of the tower. Once the floating wind turbine is subject to wind force, the response amplitudes at pitch resonant frequency and tower vibration frequency are significantly reduced. Nevertheless, response within the wave energy frequency range is somewhat amplified. It is easy to find that the response characteristics of the shaft axial force and the nacelle acceleration are very similar (see Fig. 13), manifesting that the shaft axial force is mainly induced by nacelle inertial motions.

4.5. Tower-top shear force and bending moment

Tower top is a crucial connection point of the wind turbine, in terms of limited strength and fatigue loads. As a changing point in the shape of the structure geometry, tower top is a key point for fatigue strength check as well. Therefore, the extreme values and the varying range of the shear force applied at the tower top are critical items in the dynamic response of a floating wind turbine. Statistical data of the measured shear force are listed in Table 14.

The PSD of the shear force is shown in Fig. 19, where multi-frequency components can be identified. In parked condition, shear force response is mainly dominated by three frequency components, namely the pitch resonant frequency, the wave energy frequency and the tower vibration frequency. It implies that shear force is both dominated by platform motions and tower structural dynamics. Once the wind force is considered, the shear force is diminished to a very low level at pitch resonant frequency and tower vibration frequency. Comparatively, the shear force exhibits increased response around wave energy frequency range.

Compared with the PSD curves of shear force, the PSD curves of bending moment are mainly governed by aerodynamic loads in Fig. 20 while hydrodynamic excitation and tower structural dynamics appear to have limited influence on the responses. As expected, the responses are limited in parked condition. When the wind force is considered, the bending moment is substantially excited at around 1P rotor rotation frequency (1.17 rad/s for LC2 and

Table 14
Statistical results of shear force and bending moment.

Term	Loading Case	Max	Min	Mean	Std. Dev
Shear force (kN)	LC1	753	−771	11	170
	LC2	1426	−39	796	176
	LC3	1709	316	1092	190
Bending moment (kN · m)	LC1	5003	−4485	129	1001
	LC2	2916	−12201	−4423	2812
	LC3	6117	−16503	−5957	3752

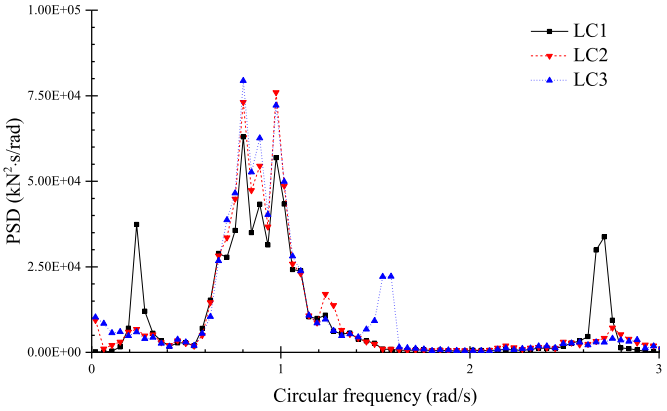

Fig. 19. Power spectrum density curves of tower-top shear force.

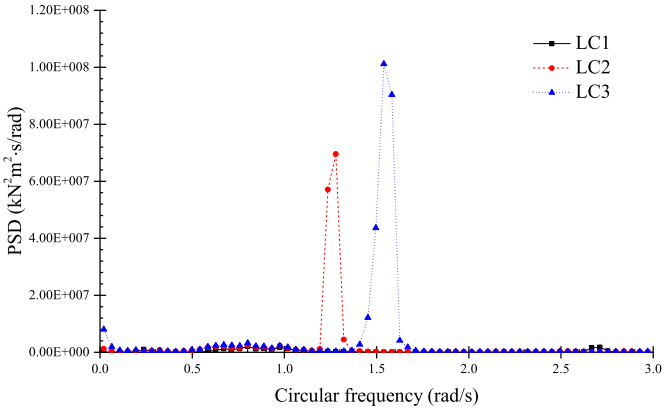

Fig. 20. Power spectrum density curves of tower-top bending moment.

1.5 rad/s for LC3) and the responses over other frequencies are nearly invisible.

4.6. Dynamic characteristics of mooring system

A floating wind turbine depends on the mooring system to maintain its position within an acceptable range. Thus, the mooring system will bear the loads induced by platform motions. The fairlead tension force of a selected mooring line is investigated in this section. Among the three mooring lines, the line along 180° direction sustains the largest load (see Fig. 5) and is therefore selected here. The statistical results of the mooring line tension are summarized in Table 15, and the corresponding PSD curves are shown in Fig. 21.

From the data in Table 15 and the curves in Fig. 21, it indicates that the tension force is mainly induced by wave force while wind force can be simplified as a linear suppression. According to the statistical data, the maximum mooring line tension increases with the thrust force. Nevertheless, the standard deviation remains relatively stable regardless of wind speed. The PSD curves demonstrate that mooring line tension is mainly wave-induced

Table 15
Statistical results of mooring line tension force (line 1).

Case No.	Max (kN)	Min (kN)	Mean (kN)	Std. dev (kN)
LC1	3981.74	1219.12	2576.42	350.94
LC2	4560.92	1673.84	3013.50	375.63
LC3	4752.02	1822.80	3188.92	375.73

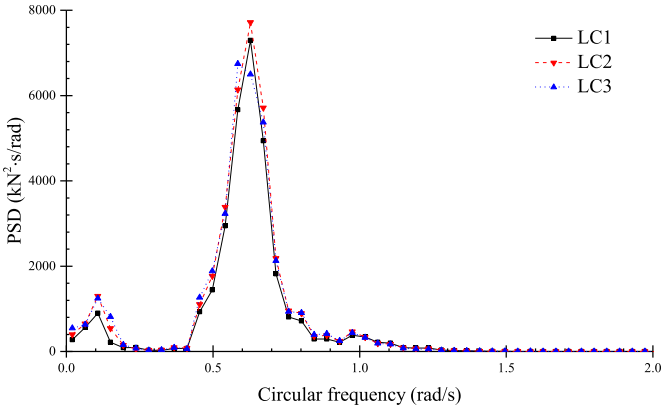

Fig. 21. Power spectrum density of mooring line tension force (line 1).

and a majority of response concentrates within wave energy frequency and resonant frequency range. Besides, little discrepancy is observed between the three curves, indicating that wind force effect is limited. It is thus reasonable to simplify aerodynamic load as an extra constant superposition when analyze mooring line dynamics. Although mooring line tension is strongly dependent on platform motions, it is interesting to find that mooring tension exhibits instinctive response characters with aerodynamic loads compared to platform motions. It inherently indicates that a static or quasi-static method (stiffness matrix model & catenary line theory) is not applicable to capture the behavior of mooring system in a numerical modeling of floating wind turbine, as both categories of methods are exactly depended on platform motions.

5. Conclusions

This paper mainly addresses the model test research of a semisubmersible floating wind turbine. A new approach is proposed in this paper to correct the deficient thrust force problem in a Froude scale experimental condition. This approach uses the wind to drive the rotor rather than using a motor. Compared with common correction ways, this approach can better simulate the operation state of the rotor and the measured shaft axial torque is more realistic. TSR can also be maintained to some extent which ensures that system excitation frequencies resulting from rotor imbalance or aerodynamic interaction with the tower will possess the correct frequency. Besides, it also overcomes some negative effects produced by common correction ways. Conclusions drawn from the study in this paper are listed in the following.

1) Platform motions suffer damping effects from the wind force and this influence is mostly effective around resonant frequency range. Although platform motions are reduced considering aerodynamic effects, nacelle accelerations are nevertheless amplified a lot at particular frequency zones by the wind force. Multi-frequency excitations are found in the response, which is dominated by the tower dynamics and the wind force.
2) The motions of a floating wind turbines exhibit distinctive features due to rotor rotation. It is observed that gyroscopic loading stimulates yaw motion even in head waves. Meanwhile, the roll resonant motion is excited by the time-varying rotor torque.
3) Tower vibration is an important item for tower-top dynamic response. In the responses of nacelle acceleration and shaft axial force, excitations have been observed around tower vibration frequency. Nevertheless, no evidence is available showing that tower dynamics has any influence on platform motion. It is also found that wind force can suppress tower vibration.

4) Shear force applied at tower top is found to be governed by multi-frequency excitation components. Shear force is excited at wave energy frequency, tower vibration frequency and rotor rotation frequency, representing hydro-aero-elastic couplings. By suppressing surge motion and tower vibration, wind force is able to reduce shear force around particular frequency range.
5) In spite of the aerodynamic effects on platform motions and tower, a selected mooring line appears to be governed by hydrodynamic loads alone and the wind force can be simplified as an extra constant force.

Acknowledgement

The authors would like to acknowledge SKLOE (State Key Lab of Ocean Engineering) in Shanghai Jiao Tong University for the model test research support. This work is also supported by China Scholarship Council (No. 201506230127).

References

[1] F.G. Nielsen, T.D. Hanson, B. Skaare, Integrated dynamic analysis of floating offshore wind turbines, in: 25th International Conference on Offshore Mechanics and Arctic Engineering, American Society of Mechanical Engineers, 2006, pp. 671–679.
[2] D. Roddier, C. Cermelli, A. Aubault, A. Weinstein, WindFloat: a floating foundation for offshore wind turbines, J. Renew. Sustain. Energy 2 (3) (2010), 033104.
[3] D. Roddier, C. Cermelli, A. Weinstein, WindFloat: a floating foundation for offshore wind Turbines—Part I: design basis and qualification process, in: ASME 2009 28th International Conference on Ocean, Offshore and Arctic Engineering, American Society of Mechanical Engineers, 2009, pp. 845–853.
[4] C. Cermelli, D. Roddier, A. Aubault, WindFloat: a floating foundation for offshore wind turbines—Part II: hydrodynamics analysis, in: ASME 2009 28th International Conference on Ocean, Offshore and Arctic Engineering, American Society of Mechanical Engineers, 2009, pp. 135–143.
[5] A. Aubault, C. Cermelli, D. Roddier, WindFloat: a floating foundation for offshore wind Turbines—Part III: structural analysis, in: ASME 2009 28th International Conference on Ocean, Offshore and Arctic Engineering, American Society of Mechanical Engineers, 2009, pp. 213–220.
[6] M. Karimirad, C. Michailides, V-shaped semisubmersible offshore wind turbine: an alternative concept for offshore wind technology, Renew. Energy 83 (2015) 126–143.
[7] L. Li, Y. Gao, Z.M. Yuan, S. Day, Z.Q. Hu, Dynamic response and power production of an integrated wind, wave and tidal energy system, Renew. Energy 116 (2017) 412–422.
[8] M. Borg, M. Collu, Offshore floating vertical axis wind turbines, dynamics modelling state of the art. Part III: hydrodynamics and coupled modelling approaches, Renew. Sustain. Energy Rev. 46 (2015) 296–310.
[9] H.R. Martin, Development of a Scale Model Wind Turbine for Testing of Offshore Floating Wind Turbine Systems, University of Maine, 2011.
[10] R. Farrugia, T. Sant, D. Micallef, A study on the aerodynamics of a floating wind turbine rotor, Renew. Energy 86 (2016) 770–784.
[11] S. Salehyar, Q. Zhu, Aerodynamic dissipation effects on the rotating blades of floating wind turbines, Renew. Energy 78 (2015) 119–127.
[12] T.J. Larsen, T.D. Hanson, A method to avoid negative damped low frequent tower vibrations for a floating, pitch controlled wind turbine, J. Phys. Conf. Ser. (2007), 012073. IOP Publishing.
[13] P.F. Odgaard, L.F. Larsen, R. Wisniewski, T.G. Hovgaard, On using pareto optimality to tune a linear model predictive controller for wind turbines, Renew. Energy 87 (2016) 884–891.
[14] J.M. Jonkman, Dynamics Modeling and Loads Analysis of an Offshore Floating Wind Turbine, University of Colorado, 2007.
[15] B. Skaare, T.D. Hanson, F.G. Nielsen, R. Yttervik, A.M. Hansen, K. Thomsen, T.J. Larsen, Integrated dynamic analysis of floating offshore wind turbines, in: European Wind Energy Conference, Milan, Italy, 2007, pp. 7–10.
[16] L. Li, Z.Q. Hu, J. Wang, Y. Ma, Development and validation of an aero-hydro simulation code for offshore floating wind turbine, J. Ocean. Wind Energy 2 (1) (2015) 1–11.
[17] S. Quallen, T. Xing, CFD simulation of a floating offshore wind turbine system using a variable-speed generator-torque controller, Renew. Energy 97 (2016) 230–242.
[18] P. Passon, M. Kühn, S. Butterfield, J. Jonkman, T. Camp, T.J. Larsen, OC3—benchmark exercise of aero-elastic offshore wind turbine codes, J. Phys. Conf. Ser. (2007), 012071. IOP Publishing.
[19] F. Vorpahl, W. Popko, IEA Wind Annex 30–OC4 project. The offshore code comparison collaboration continuation, in: IEA Wind Side Event at EWEA 2011 Annual Event, Brussels, Belgium, 2011.
[20] F. Duan, Z.Q. Hu, J.M. Niedzwecki, Model test investigation of a spar floating wind turbine, Mar. Struct. 49 (2016) 76–96.
[21] A.J. Coulling, A.J. Goupee, A.N. Robertson, J.M. Jonkman, H.J. Dagher, Validation of a FAST semi-submersible floating wind turbine numerical model with DeepCwind test data, J. Renew. Sustain. Energy 5 (2) (2013), 023116.
[22] M. Drela, XFOIL: an Analysis and Design System for Low Reynolds Number Airfoils, Low Reynolds Number Aerodynamics, Springer, 1989, pp. 1–12.
[23] J.M. Jonkman, M.L. Buhl Jr., FAST User's Guide, National Renewable Energy Laboratory (NREL), 2005.
[24] H.R. Martin, R.W. Kimball, A.M. Viselli, A.J. Goupee, Methodology for wind/wave basin testing of floating offshore wind turbines, J. Offshore Mech. Arct. Eng. 136 (2) (2014), 020905.
[25] J.M. Jonkman, S. Butterfield, W. Musial, G. Scott, Definition of a 5-MW Reference Wind Turbine for Offshore System Development, National Renewable Energy Laboratory, Golden, CO, 2009.
[26] F. Duan, Z. Hu, J. Wang, Model tests of a spar-type floating wind turbine under wind/wave loads, in: ASME 2015 34th International Conference on Ocean, Offshore and Arctic Engineering, American Society of Mechanical Engineers, 2015.